Embedded Configuration Interaction Description of CO on Cu(111): Resolution of the Site Preference Conundrum

Sahar Sharifzadeh,[†] Patrick Huang,[‡,§] and Emily Carter*[,‡]

Department of Electrical Engineering, Department of Mechanical and Aerospace Engineering, and Program in Applied and Computational Mathematics, Princeton University, Princeton, New Jersey 08544-5263

Received: November 14, 2007; In Final Form: January 11, 2008

We apply an embedded configuration interaction (ECI) theory to study the adsorption of CO on Cu(111), a well-known case where standard approximations to exchange-correlation within density functional theory (DFT) fail qualitatively to predict the correct site preference and quantitatively overbind CO to both hollow and on-top sites. In ECI theory, the chemisorption region is represented by a cluster consisting of CO and a few (4−10) nearby Cu atoms, with the effect of the periodic metallic background accounted for by an effective one-electron embedding potential derived from periodic DFT. The embedded cluster is then treated using accurate ab initio multireference configuration interaction methods for electron correlation. The ECI theory yields a CO adsorption site preference and binding energy in excellent agreement with experiment, without resorting to ad hoc corrections.

I. Introduction

Density functional theory (DFT) has proven to be a highly successful approach for describing the electronic structure of condensed matter. Although DFT can be rather accurate for the ground-state properties of nearly free-electron systems, situations exist where it fails to provide even a qualitatively correct picture, for example, strong electron−electron correlations, excited states, and open-shell systems. One well-known controversy concerns the adsorption of CO on transition-metal surfaces, where DFT does not always reproduce the adsorption site observed in experiments. Within local and semilocal approximations for exchange-correlation, DFT predicts hollow site adsorption for CO on Cu(111), Pt(111), and Rh(111),[1] but experiments consistently observe on-top site adsorption instead.[2−4]

The most extensively studied case involves CO on Pt(111). Feibelman et al.[5] reported a detailed plane-wave periodic DFT study, exploring the effects of variations in the DFT model, for example, the choice of DFT exchange-correlation, supercell, and so forth. They consistently found hollow-site adsorption to be energetically preferred. However, the treatment of Pt core states and relativistic effects has been an issue of some discussion. All-electron relativistic calculations by Olsen et al.[6] and Orita et al.[7] found a slight top-site preference. This contradicts the conclusions of Feibelman et al., who considered pseudopotential, frozen-core, and all-electron relativistic representations of core states. Although Feibelman et al. saw a stabilization of the on-top site when full-core relativistic effects are included, in their calculations this was not sufficient to switch over the CO binding site preference. In short, there are a number of technical differences between the various full-core relativistic calculations, and a careful comparative study would be needed to fully resolve the role of core relativistic effects. We note that in the case of CO on Cu(111), where relativistic effects should be negligible, all-electron DFT calculations still find a preference for hollow site adsorption, in contradiction to experiments.[8]

One explanation[1,9,10] for the general discrepancy between experiment and theory invokes the Blyholder model[11] for the transition metal−CO bond. In this picture, the highest occupied molecular orbital (HOMO) of CO (5σ) donates electrons to the metal dz^2 orbital, while the lowest unoccupied molecular orbital (LUMO) of CO ($2\pi^*$) accepts electrons from the metal $d\pi$ orbitals. For hollow site adsorption, the bonding is dominated by the CO $2\pi^*$/metal $d\pi$ interaction as a consequence of the symmetry of the CO $2\pi^*$ orbital and threefold symmetry of the hollow site. For on-top site adsorption, the CO 5σ/metal dz^2 interaction dominates. It is known that DFT underestimates the HOMO−LUMO gap (and band gaps in general) due to the self-interaction error inherent in most approximate exchange-correlation functionals. As a result, the CO $2\pi^*$ level is too low in energy, producing too strong a CO $2\pi^*$/metal $d\pi$ interaction at the hollow site. However, disagreements exist on whether the Blyholder model is too simple a picture of the metal−CO bond,[12] whether back-donation into the CO $2\pi^*$ occurs at all,[13] or whether a $2\pi^*$ resonance exists instead of back-donation.[14]

Some attempts have been made to correct the CO 5σ-$2\pi^*$ gap in DFT, in order to get the correct adsorption site for CO on transition metals. One strategy is the DFT+U method, where an additional electron−electron repulsion parameter (U-J) is introduced to shift the LUMO to higher energies.[15] Although this procedure can lead to the correct on-top site preference for CO on Cu(111), the U-J parameter is not uniquely determined in this work. Similarly, if a CI value for the CO singlet−triplet gap is used to correct DFT-GGA energies, the correct site preference for CO on a variety of transition-metal surfaces is obtained.[16]

Hybrid functionals such as B3LYP that include some fraction of Hartree−Fock exchange can also improve HOMO−LUMO gaps in molecules and insulators. Periodic B3LYP calculations

* Corresponding author. Phone: (609) 258-5391. Fax: (609) 258-5877. E-mail:eac@princeton.edu.

[†] Department of Electrical Engineering.

[‡] Department of Mechanical and Aerospace Engineering and Program in Applied and Computational Mathematics.

[§] Currently at Lawrence Livermore National Laboratory, Livermore, CA 94551.

10.1021/jp710890a CCC: $40.75
Published on Web 03/01/2008

of CO on Pt(111)[8] and Cu(111)[9] yield the correct on-top site preference in both cases. Hu et al. also found the correct on-top site preference in a B3LYP study for CO on Cu(111),[17] employing instead the ONIOM method.[18] In short, the ONIOM strategy is to locally correct the total energy in a subregion of interest. This is accomplished by carrying out a lower level calculation of the total system (in this case, periodic DFT-LDA), corrected by the energy difference between a higher level theory (here MP2 or B3LYP) and the lower level (DFT-LDA) for a finite cluster subregion. However, use of hybrid functionals containing Hartree−Fock (HF) exchange for metals is not well-justified because HF theory diverges for metallic states near the Fermi level. Nevertheless, the observation that the correct CO site preference is obtained in these various studies suggest that the problem is indeed due to the poor DFT description of the $5\sigma-2\pi^*$ gap.

An alternative approach for improving the CO $5\sigma-2\pi^*$ gap is the application of ab initio quantum chemistry methods on a cluster representing a fragment of the surface. Because cluster size effects can be significant, accounting for the extended nature of the surface is important in such calculations. An embedded quantum chemistry approach suitable for periodic, metallic crystals was developed recently,[19−25] which considers a partitioning of the total system into the periodic background and the embedded cluster containing the adsorbate. The strategy allows for the application of accurate ab initio correlation methods for the chemisorption region, in combination with a DFT-based description of the periodic background, thus overcoming the DFT band gap problem in a first-principles manner. (A thorough review of the pros and cons of other embedding methods may be found in ref 20.) Here we present results for such an embedded cluster approach to the study of CO adsorption on Cu(111). Unlike the Pt(111) case, there is no ambiguity regarding the role of core relativistic effects, which is negligible for first-row transition metals. This allows us to focus our interpretations on the role of the HOMO−LUMO gap. Earlier work[22] showed that CO excitation energies (and hence the $5\sigma-2\pi^*$ gap) are well reproduced by multireference single and double excitation configuration interaction (MRSDCI) calculations; hence, our method of choice is to employ embedded MRSDCI calculations to study CO chemisorption.

II. Embedding Theory

Details of our embedding methodology are given in ref 25. In short, the total system is partitioned into a cluster containing the adsorbate and nearby metal atoms (region I) and the periodic background (region II). The total density ρ_{tot} and energy E_{tot} are decomposed as

$$\rho_{tot} = \rho_I + \rho_{II}$$

and

$$E_{tot}[\rho_{tot}] = E_I[\rho_I] + E_{II}[\rho_{II}] + E_{int}$$

where ρ_I and ρ_{II} are densities associated with regions I and II, respectively. E_I and E_{II} denote the exact (albeit unknown) energy density functionals associated with regions I and II, and E_{int} is the unknown interaction energy between the cluster and background. We employ a DFT-based model for E_{int}

$$E_{int} = E_{tot}^{DFT}[\rho_{tot}] - E_I^{DFT}[\rho_I] - E_{II}^{DFT}[\rho_{II}]$$

where $E_i^{DFT}[\rho_i]$ (i = tot, I, II) are approximate DFT energy functionals of the form

$$E_i^{DFT} = T_s[\rho_i] + J[\rho_i] + E_{xc}[\rho_i] + \int d\mathbf{r}\rho_i(\mathbf{r})v_{ion-DFT}^i(\mathbf{r}) \quad (1)$$

Here, T_s, J, and E_{xc} are the kinetic, Hartree, and exchange-correlation energy functionals, respectively, and $v_{ion-DFT}^i(\mathbf{r})$ is the electron−ion potential. In practice, core electrons and nuclei are typically jointly represented by pseudopotentials; the subscript "ion-DFT" emphasizes that these pseudopotentials are derived from a DFT description for the isolated atom and are unscreened with DFT exchange-correlation.

The embedding approach involves recasting the total system into the form of a cluster in an effective background.[19,20,21,22,25] Given a model for E_{int}, we seek the solution of

$$\frac{\delta E_I[\rho_I]}{\delta \rho_I} + v_{emb} = 0$$

where $v_{emb} = \delta E_{int}/\delta\rho_I$ is an effective embedding potential representing the background. The Hamiltonian H_I associated with E_I is strictly ab initio in the sense that it does not rely on an approximate description for exchange and correlation; this applies as well to the electron−ion contribution to H_I, which is represented in terms of Hartree−Fock (HF) effective core potentials (ECP), $v_{ion-HF}^i(\mathbf{r})$. A DFT-type approximation is made only for the cluster-background interaction E_{int}. The density ρ_I that satisfies the previous equation can equivalently be found via the application of ab initio quantum chemistry methods to the eigenvalue equation

$$[H_I + \sum_{j=1}^{N} v_{emb}(r_j)]\,\Psi_I = E\Psi_I \quad (2)$$

where Ψ_I is a many-body wavefunction from which the density ρ_I can be derived.

The embedding potential can be written as a sum of individual contributions

$$v_{emb} = \frac{\delta E_{int}}{\delta \rho_I}$$

$$= \frac{\delta E_{tot}^{DFT}[\rho_{tot}]}{\delta \rho_{tot}} - \frac{\delta E_I^{DFT}[\rho_I]}{\delta \rho_I}$$

$$= v_{T_s}[\rho_{tot},\rho_I] + v_J[\rho_{tot},\rho_I] + v_{xc}[\rho_{tot},\rho_I] + v_{ion-DFT}^{II} \quad (3)$$

where

$$v_{T_s}[\rho_{tot},\rho_I] = \frac{\delta T_s[\rho_{tot}]}{\delta \rho_{tot}} - \frac{\delta T_s[\rho_I]}{\delta \rho_I}$$

$$v_J[\rho_{tot},\rho_I] = \frac{\delta J[\rho_{tot}]}{\delta \rho_{tot}} - \frac{\delta\, J[\rho_I]}{\delta \rho_I}$$

$$v_{xc}[\rho_{tot},\rho_I] = \frac{\delta E_{xc}[\rho_{tot}]}{\delta \rho_{tot}} - \frac{\delta E_{xc}[\rho_I]}{\delta \rho_I} \quad (4)$$

and $v_{ion-DFT}^{II}$ is the electron−ion potential due to the background region ions. Three quantities are needed to completely define the embedding potential v_{emb}: (1) an approximation for the kinetic energy T_s, (2) an approximation for the exchange-

correlation E_{xc}, and (3) a pseudopotential model for $v^{II}_{ion-DFT}$. Once specified, eq 2 is solved self-consistently for the wavefunction Ψ_I and potential v_{emb}. In the next section, we provide details on our choices for T_s, E_{xc}, and pseudopotentials and outline a procedure for a self-consistent solution of eq 2.

The total energy for the embedded cluster and background is evaluated as[20]

$$E^{emb}_{tot} = E_I + E^{DFT}_{II} + E_{int} \quad (5)$$

where $E_I = \langle \Psi_I | H_I | \Psi_I \rangle$ is computed by taking the embedded wavefunction Ψ_I from the solution of eq 2 and evaluating its energy with respect to the isolated cluster Hamiltonian H_I. We define

$$\tilde{E}^{DFT}_I = T_s[\{\varphi_n\}] + J[\rho_I] + E_{xc}[\rho_I] + \int d\mathbf{r}\rho_I(\mathbf{r})\, v^I_{ion-HF}(\mathbf{r}) \quad (6)$$

where $\{\varphi_n\}$ and ρ_I are the natural orbitals and density, respectively, associated with Ψ_I. Adding and subtracting $\tilde{E}^{DFT}_I$ to the right-hand side of eq 5 and rearranging, we get

$$E^{emb}_{tot} = \tilde{E}^{DFT}_{tot} + (E_I - \tilde{E}^{DFT}_I) \quad (7)$$

where

$$\tilde{E}^{DFT}_{tot} = \tilde{E}^{DFT}_I + E^{DFT}_{II} + E^{DFT}_{int}$$

represents a DFT energy for the total system; note, however, that underlying this definition is a HF ECP representation for the nuclei plus core electrons in region I. The $(E_I - \tilde{E}^{DFT}_I)$ term in eq 7 can be regarded as a local correction for $\tilde{E}^{DFT}_{tot}$ in region I. In this way, the embedding potential never explicitly appears in the total energy expression, though it is felt implicitly in the evaluation of the local correction because Ψ_1 and ρ_1 are optimized in the presence of v_{emb}. It is important to distinguish the local correction $(E_I - \tilde{E}^{DFT}_I)$ here from the analogous quantity in the ONIOM method.[18] In ONIOM, the wavefunction Ψ_I and density ρ_I that go into the evaluation of the local correction are obtained from a calculation for the *isolated* cluster itself, without an effective potential representing the effects of the periodic background.

The binding energy for CO on Cu(111) is defined as[21]

$$\Delta E^{emb}_{tot} = (E^{emb}_{Cu(111)} + E_{CO}) - E^{emb}_{CO/Cu(111)} \quad (8)$$

With this definition, a positive value for ΔE^{emb}_{tot} corresponds to a bound adsorbate. The quantities $E^{emb}_{Cu(111)}$, E_{CO}, and $E^{emb}_{CO/Cu(111)}$ are given in a manner analogous to E^{emb}_{tot} in eq 7 above, that is

$$E^{emb}_{CO/Cu(111)} = \tilde{E}^{DFT}_{CO/Cu(111)} + (E_{Cu_nCO} - \tilde{E}^{DFT}_{Cu_nCO})$$

$$E^{emb}_{Cu(111)} = \tilde{E}^{DFT}_{Cu(111)} + (E_{Cu_n} - \tilde{E}^{DFT}_{Cu_n})$$

$$E_{CO} = \tilde{E}^{DFT}_{CO} + (E_{CO} - \tilde{E}^{DFT}_{CO}) \quad (9)$$

$E^{emb}_{Cu(111)}$ is the energy for the *clean* Cu(111) slab, where the local correction $(E_{Cu_n} - \tilde{E}^{DFT}_{Cu_n})$ comes from an embedding calculation involving just the *clean* Cu_n cluster, that is, no adsorbate. E_{CO} is the ab initio energy for the isolated CO molecule. Substituting eq 9 into eq 8 and rearranging, we obtain

$$\Delta E^{emb}_{tot} = \Delta\tilde{E}^{DFT}_{tot} + (\Delta E_I - \Delta\tilde{E}^{DFT}_I)$$

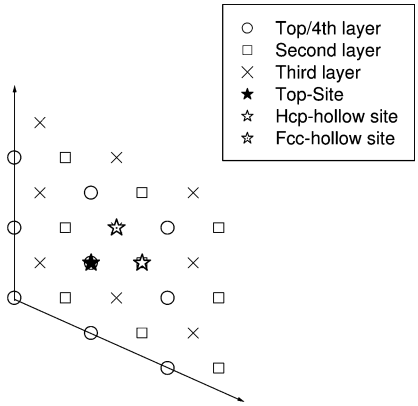

Figure 1. CO adsorption at on-top, fcc-hollow, and hcp-hollow sites of a 3 × 3 Cu(111) cell.

where

$$\Delta\tilde{E}^{DFT}_{tot} = (\tilde{E}^{DFT}_{Cu(111)} + \tilde{E}^{DFT}_{CO}) - \tilde{E}^{DFT}_{CO/Cu(111)}$$

$$\Delta E_I = (E_{Cu_n} + E_{CO}) - E_{Cu_nCO}$$

$$\Delta\tilde{E}^{DFT}_I = (\tilde{E}^{DFT}_{Cu_n} + \tilde{E}^{DFT}_{CO}) - \tilde{E}^{DFT}_{Cu_nCO} \quad (10)$$

ΔE_I and $\Delta\tilde{E}^{DFT}_I$ are the *ab initio* and DFT binding energies, respectively, for the embedded cluster; they are readily evaluated from the embedded wavefunction Ψ_I. $\Delta\tilde{E}^{DFT}_{tot}$, on the other hand, is the DFT binding energy for CO on Cu(111). It is not as straightforward to evaluate because of the presence of HF ECPs in region I. We obtain an approximation for this term via a periodic plane-wave DFT calculation for the CO/Cu(111) binding energy, using DFT pseudopotentials for both ions in regions I and II.

III. Calculational Details

A. Periodic Kohn−Sham DFT for CO on Cu(111). Periodic Kohn−Sham DFT calculations were performed for CO on Cu(111); results for both the local density approximation (LDA)[26] and generalized gradient approximation (GGA-PBE)[27] exchange-correlation functionals are reported here. The Cu(111) slab consists of four layers of Cu, and a 3 × 3 lateral supercell was employed to simulate $^1/_9$ monolayer coverage (Figure 1). The C, O, and Cu nuclei plus core electrons were represented as ultrasoft pseudopotentials.[25] The Cu(111) supercell was constructed from bulk lattice parameters of 3.57 Å (LDA) and 3.69 Å (PBE), which correspond to the equilibrium bulk Cu fcc lattice parameters associated with the underlying Cu pseudopotentials. The plane-wave basis was truncated at a kinetic energy cutoff of 1100 eV, and Brillouin zone integrations were done on a symmetrized 5 × 5 × 1 Monkhorst−Pack *k*-point mesh.[28] This choice of numerical parameters was sufficient to converge the total energy of the Cu(111) slab to within 0.01 eV/atom. All periodic DFT calculations were performed using the CASTEP plane-wave DFT code.[29]

The Cu atoms were initially placed at their bulk-terminated positions, and the positions of the CO and Cu atoms in the top two layers were subsequently optimized until the magnitude of the maximum force component acting on these atoms was below 0.05 eV/Å. Allowing for full relaxation along all directions for CO and Cu(111) produces negligible displacements of the Cu atoms relative to bulk-terminated positions and lowers the total energy of CO adsorbed on the hcp and on-top sites by only ∼0.02−0.04 eV, compared to the case where only CO coordi-

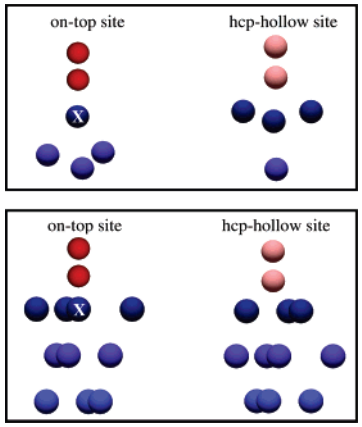

Figure 2. Cu_nCO cluster geometries. On-top and hcp-hollow site adsorption on Cu_4 and Cu_{10} clusters. The X indicates top-site Cu atom for on-top site adsorption. Atomic radii are not to scale. An additional Cu_4 cluster employed consists of the top layer of the leftmost Cu_{10} cluster.

nates were optimized. Therefore, for CO on Cu(111), we only report results where the Cu atoms were constrained to bulk-terminated positions, while CO positions were optimized along the surface normal. Geometry relaxation of the clean Cu(111) slab lowered its total energy by only 0.01 eV; therefore, the bulk-terminated geometry was always used for Cu(111). Moreover, the difference between the DFT hcp- and fcc-hollow site adsorption energies for both LDA and GGA-PBE calculations was 0.02 eV or less, and so we focus only on the hcp-hollow site for reasons of computational convenience. The optimized gas-phase CO bond length (LDA: 1.122 Å; GGA: 1.132 Å; experiment:[30] 1.128 Å) and surface−CO distance (LDA: 1.85 Å; GGA: 1.92 Å; experiment:[31] 1.91 Å) are in reasonable agreement with experiment.

B. Multireference Single and Double Excitation Configuration Interaction (MRSDCI) Calculations for Bare Cu_nCO Clusters. Bare cluster calculations were done for Cu_n clusters ($n = 4, 10$) representing a fragment of the Cu(111) slab and for the corresponding Cu_nCO clusters (Figure 2). We selected clusters with an even number of Cu atoms to allow for the possibility of a nonmagnetic electronic structure as in bulk Cu. The Cu_4 and Cu_4CO clusters possess C_{3v} point group symmetry, whereas Cu_{10} and $Cu_{10}CO$ have C_3 symmetry. The number of Cu atoms per surface layer (a, b, c) for each cluster is (1, 3, 0), (3, 1, 0), (4, 3, 3), and (3, 4, 3) for Cu_4-top, Cu_4-hcp, Cu_{10}-top, and Cu_{10}-hcp, respectively. Here, a, b, and c denote the number of Cu atoms in the top, second, and third surface layers, respectively. Positions for Cu_n were kept at the bulk-terminated DFT-LDA Cu(111) values, whereas the positions for CO in the gas and adsorbed phases were taken from the geometry optimized DFT-LDA values. The LDA optimized geometries were used rather than the GGA ones for consistency with subsequent embedding calculations, which involve an embedding potential derived from the LDA. Because the valence band of Cu(111) is nearly free-electron-like, LDA should give a good description of the background. HF ECPs were employed to represent the nuclei plus core electrons of the clusters, while Gaussian basis sets optimized for use with these ECPs were employed for the valence electrons. The C and O ECPs[32] include the 1s shell as core and regard the 2s2p shells as valence. For the top layer Cu atoms, the ECPs[33] include shells up to 3s and 3p as core, and treat 3d4s as valence. Beyond the first layer, Cu 3d electrons are not expected to play an active role in the metal−CO bond, and thus the remaining Cu atoms are modeled with large core ECPs[34] where the 3d shell is also subsumed into the core, leaving only the 4s as valence.

The MRSDCI[35] method was applied to the Cu_nCO ($n = 4$, 10) clusters, and binding energies were evaluated relative to a Cu_nCO supermolecule with the CO and Cu_n cluster over 20 Å apart. The MRSDCI method forms a configuration interaction (CI) expansion from single and double excitations out of a set of dominant reference configurations. Use of a supermolecule approach to calculate binding energies renders MRSDCI size-consistent though not size-extensive. For systems of the size under investigation, size extensivity errors are expected to be small. Input molecular orbitals and choice of reference configurations for MRSDCI calculations were generated by the complete active space self-consistent field (CASSCF) method[36] for $n = 4$ clusters or the restricted active space self-consistent field (RASSCF) method[37] for $n = 10$ clusters.

The CASSCF method is a full CI expansion within a prescribed set of valence electrons and orbitals (the active space) where the orbitals and CI coefficients are both variationally optimized. CASSCF captures static correlation by mixing near-degenerate electron configurations. We used an active space of 10 electrons in 8 orbitals for CO, which was found to be sufficient,[22] and 1 electron per orbital for each Cu atom (i.e., the Cu 4s) for our CASSCF calculations. For $n = 10$, a CASSCF active space constructed in an analogous manner was not computationally feasible and therefore the RASSCF method was used. Instead of a full CI in an active space, RASSCF limits the excitation order while still optimizing both CI and orbital coefficients. Here, we carry out an MRSDCI-SCF as our RASSCF.

We chose to include within the RASSCF active space all orbitals and electrons that can potentially contribute to the CO/Cu(111) bond. Because CO may bond to Cu d orbitals near the adsorption site or to the s band of Cu(111), the active space should in principle include all CO valence electrons, all Cu s electrons, and all d electrons on the Cu atom(s) adjacent to the adsorption site. Although the inclusion of all such electrons in the active space is most likely unnecessary, we prefer not to have any a priori bias as to which ones are required and which are not. Thus, for top-site adsorption, we should include in our MRSDCI-SCF active space all orbitals and electrons associated with CO, the Cu s band, and the top-site Cu d orbitals. Similarly, to describe hcp-hollow site adsorption properly, we should include all orbitals and electrons associated with the CO, the Cu s band, and the three sets of Cu d orbitals associated with Cu atoms adjacent to the adsorption site. However, we find that the CO 3σ orbital and one low-energy orbital of Cu sp character are unnecessary to include in the active space because they remain essentially doubly occupied in the RASSCF wavefunction when included (with occupation numbers of 1.992 and 1.996, respectively). Therefore, instead we include CO 4σ, 1π, 5σ, as many of the desired Cu orbitals and an equal number of corresponding empty correlating orbitals as is computationally possible. When the ground-state wavefunctions of the Cu_{10} or $Cu_{10}CO$ clusters are closed-shell, only one reference state dominates and therefore the CI involves single and double excitations from that single reference configuration only. When the ground-state wavefunctions of the Cu_{10} or $Cu_{10}CO$ clusters contain in their dominant configurations two open-shell electrons distributed over two orbitals, these two orbitals define the multi-(three) reference states from which single and double excitations are allowed. For on-top site calculations, all desired occupied and correlating orbitals could be included: 26 electrons in 26 orbitals. For closed-shell clusters, the active space contains 13 strongly (nearly doubly) occupied CO and Cu_{10} orbitals and 13

correlating orbitals; for open-shell clusters, the active space consists of two Cu_{10} orbitals defining the multireference states, 12 strongly occupied CO and Cu_{10} orbitals and 12 correlating orbitals. For hcp site calculations, it was feasible to include only 22 electrons in 22 orbitals. For closed-shell clusters, the active space consisted of 11 strongly occupied CO and Cu_{10} orbitals and 11 corresponding correlating orbitals; for open-shell systems, the active space consisted of the two Cu_{10} orbitals defining the multireference state, 10 strongly occupied CO and Cu_{10} orbitals and 10 corresponding correlating orbitals. Although not all of the desired orbitals are contained within the RASSCF active space, here RASSCF is used only to generate input orbitals and to identify the important reference configurations for subsequent MRSDCI calculations. Test calculations on Cu_4-CO comparing RASSCF and CASSCF orbitals and CI coefficients show little difference in the resulting MRSDCI total energy (<0.02 eV), suggesting that the RASSCF wavefunction will provide an adequate starting point for the subsequent MRSDCI calculations.

Because of the large number of electrons in these clusters, it is also necessary to limit the number of correlated electrons and/or number of reference states within the MRSDCI calculations. In order to evaluate the best course of action, tests were performed where the number of correlated electrons and number of reference configurations were varied. These results are discussed in detail in Section IV.

All ab initio cluster calculations were performed using a modified version of the MOLCAS package,[38] MOLCAS-embed.

C. ONIOM Correction to Periodic Kohn−Sham DFT. For comparison with other studies,[17] we also report adsorption site preferences and binding energies using the ONIOM correction, evaluated as

$$E_{\mathrm{tot}}^{\mathrm{ONIOM}} = E_{\mathrm{tot}}^{\mathrm{DFT}} + (E_{\mathrm{I}} - E_{\mathrm{I}}^{\mathrm{DFT}})$$

where $E_{\mathrm{tot}}^{\mathrm{DFT}}$ is obtained from the periodic plane-wave DFT calculation for CO/Cu(111), and E_{I} and $E_{\mathrm{I}}^{\mathrm{DFT}}$ come from ab initio and DFT calculations with HF ECPs for the isolated region I cluster ($v_{\mathrm{emb}} = 0$), respectively. Note that this is not the same as $E_{\mathrm{tot}}^{\mathrm{emb}}$ in eq 7, where the correction terms are evaluated using wavefunctions derived from an embedded cluster calculation. To compute $E_{\mathrm{I}}^{\mathrm{DFT}}$ for the cases where the cluster wavefunction was an open-shell singlet, unrestricted DFT was applied.

The DFT calculations are performed using the modified version of the MOLCAS package,[38] MOLCAS-embed.

D. Embedded Cluster: Specification of v_{emb}. For calculations involving the embedding formalism of Section II, two approximations for the kinetic energy potential, eq 4, were considered: the Thomas−Fermi $^1/_9$-von Weizsäcker model[39]

$$\frac{\delta T_{\mathrm{s}}[\rho_{\mathrm{tot}}]}{\delta \rho_{\mathrm{tot}}} - \frac{\delta T_{\mathrm{s}}[\rho_{\mathrm{I}}]}{\delta \rho_{\mathrm{I}}} = \left(\frac{\delta T_{\mathrm{TF}}[\rho_{\mathrm{tot}}]}{\delta \rho_{\mathrm{tot}}} + \frac{1}{9}\frac{\delta T_{\mathrm{vW}}[\rho_{\mathrm{tot}}]}{\delta \rho_{\mathrm{tot}}}\right) - \left(\frac{\delta T_{\mathrm{TF}}[\rho_{\mathrm{I}}]}{\delta \rho_{\mathrm{I}}} + \frac{1}{9}\frac{\delta T_{\mathrm{vW}}[\rho_{\mathrm{I}}]}{\delta \rho_{\mathrm{I}}}\right) \quad (11)$$

and an orbital-based model[25]

$$\frac{\delta T_{\mathrm{s}}[\rho_{\mathrm{tot}}]}{\delta \rho_{\mathrm{tot}}} - \frac{\delta T_{\mathrm{s}}[\rho_{\mathrm{I}}]}{\delta \rho_{\mathrm{I}}} = \left(-\frac{1}{2}\gamma \sum_i \frac{\psi_i^* \nabla^2 \psi_i}{\rho_{\mathrm{tot}}}\right) - \left(-\frac{1}{2}\gamma \sum_j \frac{\varphi_j^* \nabla^2 \varphi_j}{\rho_{\mathrm{I}}}\right) \quad (12)$$

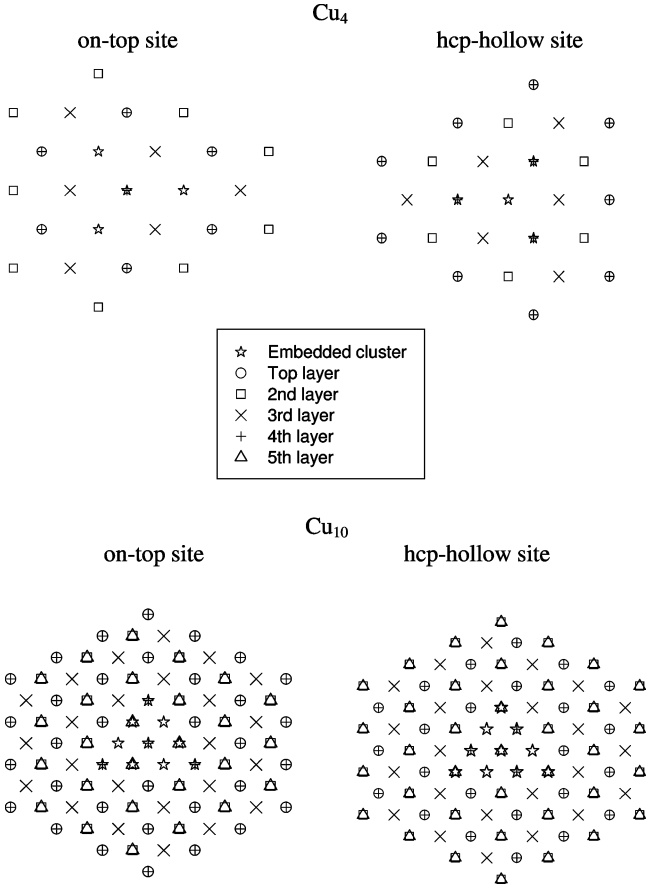

Figure 3. Positions for nonlocal pseudopotential centers for Cu_4 and Cu_{10} clusters. Convergence with respect to changes in the embedded wavefunction determined the number of centers required.

In the latter definition, $\{\psi_i\}$ and ρ_{tot} are the orbitals and density, respectively, obtained from a plane-wave Kohn−Sham DFT calculation for the total CO/Cu(111) system. Similarly, $\{\varphi_j\}$ and ρ_{I} are the orbitals and density from a plane-wave Kohn−Sham DFT calculation for the *isolated* Cu_nCO cluster. The parameter γ is an adjustable nonlinearity parameter set to 0.8; this choice was made based on DFT-in-DFT embedding tests for a Cu dimer in Cu(111).[25] For embedding calculations employing kinetic energy in the form of eq 12, this quantity must be evaluated once and held frozen at its initial value; that is, it is not self-consistently updated along with all the other terms in the embedding potential.

The electron−ion contribution to the embedding potential due to the background, $v_{\mathrm{ion}}^{\mathrm{II}}$, is given by norm-conserving pseudopotentials constructed to be consistent with the ultrasoft pseudopotentials used in the plane-wave DFT calculations.[25] These pseudopotentials consist of a long-range Coulombic ($-Z_{\mathrm{val}}/r$) term and short-range nonlocal contributions. The Coulombic term is evaluated in reciprocal space, whereas the nonlocal terms are evaluated in real space. Therefore, a finite number of ion centers have to be explicitly defined in real space for the nonlocal terms, which are shown in Figure 3. In all cases, we have checked that an increase of the number of nonlocal pseudopotential centers does not change the embedded wavefunction. The number of nonlocal pseudopotential centers per layer is (6, 9, 6, 7, 0), (9, 6, 6, 12, 0), (33, 24, 24, 37, 27), and (24, 33, 24, 27, 37) for Cu_4-top, Cu_4-hcp, Cu_{10}-top, and Cu_{10}-hcp, respectively. This corresponds to a total number of 28 (Cu_4-top), 33 (Cu_4-hcp), 145 (Cu_{10}-top), and 145 (Cu_{10}-hcp) centers.

The exchange-correlation contribution to the embedding potential, v_{xc}, is computed using the local density approximation

(LDA), which is consistent with the plane-wave DFT calculations. The valence electrons of Cu, the 4sp band, are nearly free-electron-like and therefore are well-described by the LDA.

The Hartree contribution to the embedding potential, v_J, is computed exactly in reciprocal space.[20]

E. Embedded Cluster: Self-Consistent Solution. Once the embedded cluster is chosen, an estimate for the background density ρ_{II} is made. Two estimates for ρ_{II} were considered. The first is the difference density

$$\rho_{II} = \rho_{tot}^{DFT} - \rho_{I}^{DFT} \quad (13)$$

where ρ_{tot}^{DFT} is obtained from a plane-wave DFT calculation for the clean Cu(111) slab and ρ_{I}^{DFT} comes from a plane-wave DFT calculation for the isolated Cu_n cluster. The second is a notched surface density $\rho_{II} = \rho_{II}^{notched}$, which is obtained from a plane-wave DFT calculation for the background region alone. We investigate both possibilities. ρ_{II} is the density associated with a set of background atoms; this set contains all atoms (with the exception of those contained in region I) of either the four-layer, 3×3 supercell for the $n = 4$ clusters or the five-layer, 8×8 supercell for the $n = 10$ clusters. We increase the background size for the $n = 10$ cluster in order to avoid the cluster interacting with its periodic image. The difference density method for constructing ρ_{II} has the advantage that it can be constructed from an inexpensive primitive cell calculation for the metal surface for ρ_{tot}^{DFT} by simply extending the primitive cell densities to construct a larger supercell.[40]

Once ρ_{II} is constructed, it is kept fixed throughout the embedding calculation. An initial guess for $v_{emb}[\rho_{tot}^{(0)},\rho_{I}^{(0)}]$ is first constructed, where $\rho_{I}^{(0)}$ is initially taken to be the bare region I cluster CASSCF/RASSCF density, and in general $\rho_{tot}^{(n)} = \rho_{I}^{(n)} + \rho_{II}$. A new embedded cluster wavefunction $\Psi_{I}^{(1)}$ and its associated density $\rho_{I}^{(1)}$ is found from CASSCF or RASSCF calculations in the presence of this $v_{emb}[\rho_{tot}^{(0)},\rho_{I}^{(0)}]$, and an updated $v_{emb}[\rho_{tot}^{(1)},\rho_{I}^{(1)}]$ is evaluated accordingly. This procedure is repeated until self-consistency is reached. Once the converged CASSCF/RASSCF embedding potential is found, an MRSDCI calculation is performed in the presence of this potential. This calculation produces the embedded wavefunction from which energies E_I and $\tilde{E}_{I}^{DFT}$ as described in eqs 5−7 are obtained.

F. Embedded Cluster: Calculation of $\tilde{E}_{I}^{DFT}$. As discussed earlier, $\tilde{E}_{I}^{DFT}$ is computed from natural orbitals of the embedded MRSDCI wavefunction. The natural orbitals are kept frozen, and the DFT energy is computed using integer occupation of orbitals, as appropriate for a ground-state DFT calculation. Because the natural orbitals of MRSDCI wavefunctions are fractionally occupied, by integer occupation of orbitals we mean that all strongly occupied orbitals are given occupation number 2, all weakly occupied orbitals are assigned occupation number 0, and singly occupied orbitals have occupation number 1. For the cases in which the clusters are open-shell singlets, the DFT energy is computed using unrestricted DFT.

IV. Results and Discussion

We examined CO adsorption on Cu(111) and compared results from four different models: (1) periodic slab DFT, (2) MRSDCI calculations for CO on bare Cu_n clusters representing fragments of Cu(111), (3) a local correction to the periodic slab DFT results via the ONIOM scheme, and (4) MRSDCI calculations for embedded Cu_nCO. The theoretical predictions were compared to experimental measurements, where a number of studies for CO on Cu(111) at low coverage have been reported. The observed low-energy electron diffraction (LEED) pattern is consistent with on-top site adsorption, and CO binding energies of 0.45−0.52 eV have been derived from temperature-programmed desorption (TPD).[2,41−44]

TABLE 1: Binding Energies (eV) for Top- and hcp-Site Adsorption of CO on Cu(111), Evaluated from Periodic Slab DFT, Bare Cu_nCO ($n = 4$, 10) Cluster MRSDCI Theory, an ONIOM Correction to the Periodic Slab DFT, and Embedded MRSDCI Theory[a]

	on-top site		hcp site	
CO/Cu(111), LDA	1.24		1.54	
CO/Cu(111), PBE	0.65		0.75	
expt[2,41,42,43,44]	0.45−0.52			
	Cu_4CO	$Cu_{10}CO$	Cu_4CO	$Cu_{10}CO$
bare cluster MRSDCI	0.50 (−0.59)	0.33	−0.40	−0.66
ONIOM MRSDCI-LDA	0.94 (0.42)	0.63	0.058	−0.11
embedded MRSDCI	0.67 (0.48)	0.49	−0.10	−0.092

[a] The binding energy is defined such that it is positive for a bound adsorbate. Values in parentheses are the binding energies of CO to a Cu_4 cluster with four top-layer Cu atoms (see text for details).

A. Periodic Kohn−Sham DFT Calculations. As expected, the periodic DFT calculations yield a preference for hollow site adsorption, in disagreement with experiment (Table 1). In addition to the typical overbinding at the LDA level, even GGA overbinds CO compared with experiment. As discussed in the Introduction, DFT-LDA and GGA underestimate the CO $5\sigma-2\pi^*$ gap, leading to a preference for hollow site binding, thus motivating an ab initio description of the metal−CO bond.

B. Bare Cluster MRSDCI Calculations and ONIOM Corrections. CASSCF/RASSCF and MRSDCI calculations were performed for the isolated Cu_nCO cluster ($n = 4$, 10), and binding energies were obtained relative to the Cu_n/CO supermolecule. The binding energy is reported only at the MRSDCI level because dynamical correlation is critical to describe the weak bonding of CO to Cu, where dispersion forces also play a nontrivial role.

For $n = 4$ and 10, both Cu_n and Cu_nCO have triplet ground states, with the two triplet-coupled electrons distributed over Cu orbitals of sp character. Such a triplet ground state for Cu_4 and CO adsorbed on top-site of Cu_4 was also predicted in CI calculations by Mochizuki et al.[45] However, because we aim to model CO adsorption on the nonmagnetic Cu(111) surface, we report binding energies with respect to the lowest-energy singlet state of each cluster. For $n = 4$, the clean Cu_4 clusters used to model both top- and hcp-site adsorption have identical Cu−Cu relative positions (Figure 2). However, as described in Section III, the ECPs and basis sets describing the Cu atoms at the chemisorption site differ from the other Cu atoms. The Cu_4 cluster employed for top-site adsorption has one Cu at the chemisorption site, while the hcp cluster has three Cu. In both cases, for the clean Cu_4 clusters, we find two electrons distributed over an a_1 and an $\{e_x, e_y\}$ set of orbitals of Cu sp character, forming a set of doubly degenerate ^1E states and a nondegenerate $^1A_1$ state that are all close in energy (within 0.2 eV). The lowest singlet state of the Cu_4 top-site cluster is $^1A_1$, while for the hcp-site cluster the lowest singlet is ^1E. Adding the CO molecule yields an open-shell ^1E as the lowest singlet state for both top- and hcp-site clusters, with the open-shell electrons distributed over $\{e_x, e_y\}$ orbitals of Cu sp character. For $n = 10$, the lowest-energy singlet states for the $Cu_{10}CO$ clusters are doubly degenerate ^1E states, with the two open-shell electrons distributed over a set of $\{e_x, e_y\}$ orbitals. For on-top adsorption, this set of orbitals $\{e_x, e_y\}$ are of Cu sp character, while for hcp-site adsorption, this set of orbitals are

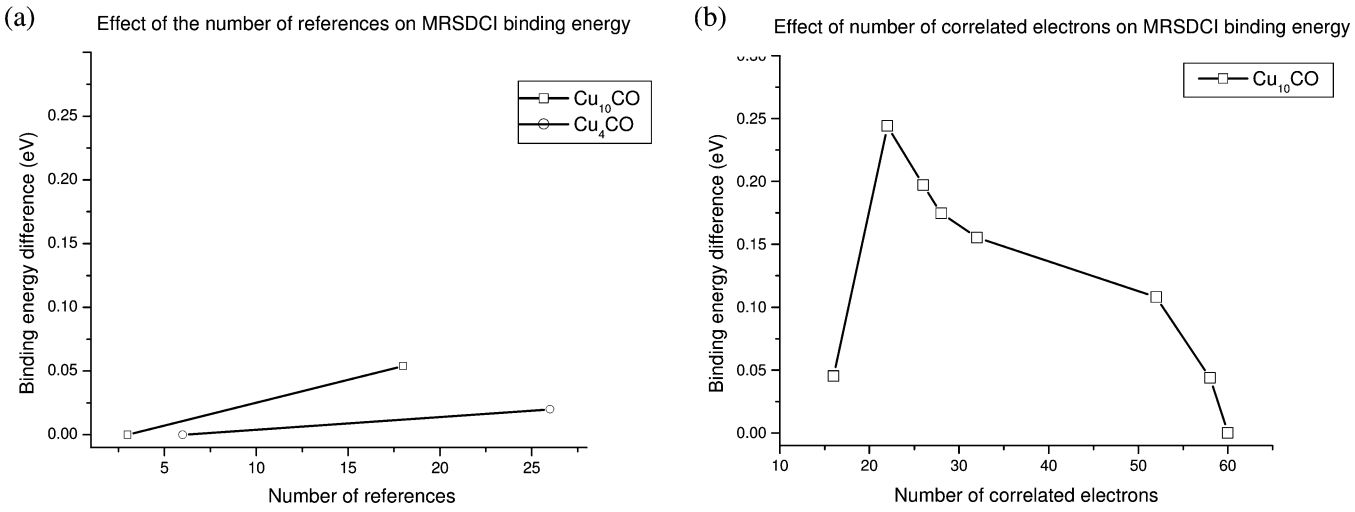

Figure 4. MRSDCI expansion tests for top-site CO adsorption on bare Cu_n. (a) The effect of increasing the number of references on the Cu_nCO binding energy. The two data points for each cluster correspond to inclusion of reference configurations with CASSCF coefficients >0.1 and >0.05 ($n = 4$) and or RASSCF coefficients >0.1 and >0.04 ($n = 10$). The number of correlated electrons are 14 and 16 for $n = 4$ and 10, respectively. (b) The effect of leaving some electrons uncorrelated on $Cu_{10}CO$ binding energy. The same number of reference configurations (those with RASSCF coefficients >0.1) were included in all calculations. We conclude that to achieve highest accuracy it is necessary to correlate all valence electrons, whereas use of reference configurations with coefficients >0.1 is sufficient.

composed of a mixture of Cu sp and CO π character. For the two clean Cu_{10} clusters, the lowest-energy singlet state is a ^1E state for the on-top site cluster, with the doubly degenerate electrons distributed over $\{e_x, e_y\}$, while the lowest-energy singlet state for the hcp-site cluster is a $^1A_1$ state.

Figure 4 shows the results of CI expansion tests for the binding energy of CO adsorbed at the on-top sites of Cu_4 and Cu_{10}. The specification of a MRSDCI wavefunction involves two choices: the number of reference configurations out of which single and double excitations are generated and the number of correlated/uncorrelated electrons. We use the term "correlated" here to refer to electrons that occupy different orbitals in the CI expansion, while "uncorrelated" or "frozen" refer to electrons that doubly occupy the same orbital in all configurations. In order to assess the necessary number of reference configurations, we first fixed the number of correlated electrons at 14 for $n = 4$ and 16 for $n = 10$ and varied the number of references (Figure 4a). References were taken from CASSCF/RASSCF wavefunctions by selecting configurations with CI coefficients $c \geq |0.1|$; the number of references was then increased by lowering this threshold to $c \geq |0.05|$ for $n = 4$ and $c \geq |0.04|$ for $n = 10$. The CO binding energy changed by a very small amount ($\leq$0.05 eV) as the number of reference configurations was increased.

In contrast, Figure 4b shows that the CO binding energy is strongly affected by a decrease in the number of correlated electrons. Here we exhibit how the CO binding energy to Cu_{10} is affected, when only reference configurations with coefficients $c \geq |0.1|$ within RASSCF are included, and the number of correlated electrons is systematically decreased. The first two electrons we freeze correspond to the CO 3σ electrons, which contribute negligibly to the Cu_n−CO bonding. When the number of correlated electrons is 28, all electrons that we expect to contribute to the bond (all CO electrons other than 3σ, all top-site Cu *d*-electrons, and all Cu *s*-electrons) are correlated, while the d electrons of Cu atoms for atoms adjacent to the binding site are kept frozen. In this case, CO binding energy changed by 0.25 eV. This indicates that the correlation of all Cu electrons is much more crucial within our calculations than the inclusion of many reference configurations. Even though these orbitals may not contribute obviously to the bonding, they contribute to describing polarization of the Cu_n cluster. Similar tests performed for hcp site adsorption lead to the same conclusions. Therefore, the final MRSDCI calculations include reference configurations with coefficients $c \geq |0.1|$ within CASSCF or RASSCF, and all valence electrons are correlated within MRSDCI for all clusters except for CO adsorption on the hcp site of Cu_4, where the CO 3σ was not. This was necessary because of the large number of reference configurations required for this system; moreover, we have shown that CO 3σ has a negligible effect on the binding energy, so there is no need to include it here.

In order to calculate the ONIOM energy as described in Section III, we must calculate the DFT energy of the cluster. We calculated the DFT energy of the clusters using unrestricted DFT, in order to allow for the formation of an open-shell singlet as was seen with MRSDCI. However, the wavefunctions could only be converged to symmetry-broken closed-shell wavefunctions in all cases; we report numbers with respect to these results.

In Table 1, we compare binding energies for bare (not embedded) Cu_nCO calculations within MRSDCI and local corrections to periodic DFT via the ONIOM approach. In contrast to periodic DFT, both MRSDCI cluster calculations and the ONIOM approach predict top-site adsorption. This is due to an improved description of the CO $2\pi^*$ level with MRSDCI. However, for $Cu_{10}CO$, the CO binding energy to the isolated cluster from MRSDCI (0.33 eV) and from the ONIOM approach (0.63 eV) deviate from the experimental value (0.45−0.52 eV). Moreover, the binding energies for both the top and hollow site are not converged with respect to cluster size for either method at Cu_{10}.

C. Embedded MRSDCI Calculations. Embedded MRSDCI calculations with an LDA embedding potential were performed for Cu_nCO and Cu_n/CO supermolecules. As with the bare cluster, we report binding energies for the lowest-energy singlet state and we optimize the embedding potential and wavefunction with respect to the singlet. The embedding potential stabilizes the singlet state relative to the triplet (as it should, given that an extended Cu surface is nonmagnetic). For embedded Cu_4-CO and Cu_4 clusters, the singlet and triplet states are nearly degenerate, whereas for embedded $Cu_{10}CO$ and Cu_{10}, the ground states are singlets. Already then, we see an improved representa-

tion of the Cu surface via the embedding theory as compared to bare cluster or ONIOM calculations because we find singlet ground states for the Cu substrate model. For Cu_nCO ($n = 4$, 10), the symmetries of the lowest singlet states are the same as for the bare clusters. For the top-site Cu_4 embedded cluster, the lowest singlet state is a doubly degenerate ^1E state, where the two open-shell, singlet-coupled electrons are distributed over a_1 and $\{e_x, e_y\}$ orbitals of Cu sp character. For the hcp-site Cu_4 embedded cluster, the lowest-energy singlet state is a closed-shell $^1A_1$. For both the on-top and hcp-hollow site Cu_{10} embedded clusters, the ground states are closed-shell $^1A_1$ states. In order to gain insight into the nature of the Cu surface−CO bond, we look at the RASSCF natural orbitals of the embedded Cu_nCO system and how they change character as the CO molecule is brought to the surface. Although we see mixing of both CO σ and π with Cu sp states, the σ-mixing dominates for on-top adsorption, while π-mixing dominates for hcp site adsorption. This confirms the idea that the CO 5σ interaction is of primary importance for on-top site adsorption whereas π-backbonding is primary for hcp-site adsorption.

The choice for the frozen background density ρ_{II} and the kinetic energy component T_s of the embedding potential in principle are critical features of the model that should be tested. We looked at their effects on the CO binding energy for Cu_4-CO (Figure 2) and Cu_6CO at the CASSCF level. The Cu_6 cluster has three atoms per layer, (3, 3, 0) in the earlier nomenclature, and is a convenient choice because the same cluster can be used to model on-top and hcp site adsorption. We do not report CO binding energies on this cluster because it breaks the surface three-fold symmetry and CO π symmetry; nevertheless, this cluster is useful for examining the role of ρ_{II} and T_s. The background density corresponds to a four-layer Cu(111) 3×3 supercell and CASSCF calculations are performed with 10 electrons in 8 orbitals for CO and n electrons in n orbitals for Cu_n ($n = 4$, 6). Embedded CO binding energies using background densities as defined in eq 13 or as $\rho_{II} = \rho_{II}^{notched}$ differed by ≤ 0.1 eV. Similarly, given a definition of the frozen background density, $\rho_{II} = \rho_{tot}^{DFT} - \rho_{I}^{DFT}$, varying the kinetic energy component of the embedding potential between the non-self-consistent orbital-based and orbital-free functionals produced a CO binding energy difference of only 0.1 eV. For our final calculations, then, we chose to use $\rho_{II} = \rho_{tot}^{DFT} - \rho_{I}^{DFT}$ and the self-consistent orbital-free kinetic energy.

We performed MRSDCI calculations in the presence of the converged CASSCF/RASSCF embedding potential to get an embedded wavefunction and evaluated binding energies as described in eq 10 for embedded Cu_nCO ($n = 4$, 10) and associated supermolecules. The CASSCF/RASSCF active spaces are the same as given in Section III and the MRSDCI calculations correlate all valence electrons and include reference configurations with coefficients $c \geq |0.1|$ for all clusters.

Table 1 displays CO binding energies obtained with embedded MRSDCI theory. As with the isolated cluster calculations, embedded cluster calculations yield the correct preference for on-top site adsorption by providing via MRSDCI a correct description of the CO $2\pi^*$ level, which then disfavors hcp site adsorption. Unlike the isolated cluster MRSDCI or ONIOM calculations, however, the predicted CO binding energy on embedded Cu_{10} (0.49 eV) is in excellent agreement with experiment. Moreover, we see that the embedded MRSDCI predictions for CO *non-binding* to the hcp site are converged with respect to cluster size to within 0.01 eV, even at Cu_4, again in excellent agreement with the observed absence of CO hollow site binding. We believe this fast convergence with respect to cluster size is due to the presence of the embedding potential, which minimizes the finite size effects seen in bare clusters.[22] However, the on-top site adsorption energies do not show the same full convergence with cluster size. Examination of the cluster morphology suggests that the origin of changes in the adsorption energy for the on-top site may be the presence of only one surface Cu atom for the on-top site Cu_4 cluster. It seems plausible that our assumption that the background density in region II is unaffected by changes in region I may not be valid in this case. It is likely that a minimum of three surface layer Cu atoms are required for this assumption to be valid; other embedding calculations for chemisorption on Cu surfaces support this suggestion.[24,25,40] This is also supported by the rapid cluster size convergence seen with hcp site adsorption, for which the clusters all have three top layer atoms. Thus it is likely that the embedded $Cu_{10}CO$ cluster offers a good description of CO/Cu(111) because four top layer atoms are used to represent the surface.

In order to test the importance of including more Cu surface atoms in the embedded cluster, we carried out embedded MRSDCI calculations on a different Cu_4 cluster: we took the top layer of the Cu_{10} cluster shown in Figure 2 (bottom left), which contains four surface Cu atoms. If this cluster gives binding energies that agree with the Cu_{10} binding energies, then we will have shown what is necessary to achieve convergence of adsorption energies. Of course, we would have preferred to go to even larger clusters of Cu beyond Cu_{10} to further prove convergence, but the prohibitive cost of MRSDCI precludes this route.

CO binding energies to the two-dimensional Cu_4 (subset of Cu_{10}) cluster are also given in Table 1 (in parentheses) for embedded MRSDCI, isolated cluster MRSDCI, and the ONIOM approach. We see that the embedded MRSDCI value (0.48 eV) is in excellent agreement with both the embedded MRSDCI value for Cu_{10} above and experiment. We therefore conclude, to the best of our ability to do so, that the embedded CI results are converged with respect to cluster size. In contrast, the isolated cluster MRSDCI and ONIOM calculations do not show convergence of binding energy with respect to cluster size. MRSDCI calculations on this cluster find CO to be unbound, and ONIOM calculations show a 0.2 eV difference in binding energy compared to ONIOM applied to the Cu_{10} cluster.

In principle, MRSDCI on a sufficiently large bare metal cluster should give the correct binding energies. The trouble is that very large (~100 atom) clusters would be required, much larger than can be treated with CI, in order to represent properly an extended metal surface (due to its inherently delocalized electronic structure). In contrast, small metal clusters suffer from edge effects that make them poor models for an extended surface. This is evident in Table 1, where CO binding energies are still not converged for the $N = 10$ bare cluster models. CO binding energies from the embedded clusters, however, are converged at $N = 10$, demonstrating that the embedding eliminates the edge effects and allows convergence of local properties such as chemisorption at cluster sizes amenable to CI.

V. Conclusions

Our goal in this work was to apply a theory with no ad hoc corrections or inappropriate physics that would reveal whether an ab initio method could reproduce the correct chemisorption binding site of CO on a transition-metal surface, which standard forms of DFT fail to do. The failure is due to self-interaction error within standard DFT, which yields too low a $2\pi^*$ level

for CO and therefore overemphasizes dπ backbonding to CO, which overstabilizes hollow site adsorption, contrary to experiment where hollow site adsorption is not observed. Earlier work has only been able to obtain the correct binding site (and sometimes binding energy) by resorting to either empirical corrections or methods that we believe give the right answer for the wrong reason, namely, any method that employs Hartree−Fock theory (e.g., B3LYP, with or without ONIOM) to describe a metal. Instead, we applied our embedded MRSDCI theory to this problem, which has a correct description of both the extended Cu(111) crystal via a periodic embedding potential and a correct description of the metal−CO bond and CO $2\pi^*$ level. We compared our results to standard periodic DFT, bare cluster MRSDCI, and the ONIOM correction to periodic DFT. As expected, DFT predicts hollow site adsorption with too high a binding energy. MRSDCI (with a bare cluster to represent atoms near the adsorption site, with ONIOM theory, or with embedding theory) predicts the correct binding site due to a high-quality ab initio description of the CO $2\pi^*$ level. Moreover, the embedding theory predicts a CO binding energy in excellent agreement with experiment and greater stability of binding energy with respect to change in cluster size (when compared with bare cluster MRSDCI or ONIOM theory). Last, unlike in periodic DFT, which predicts that CO should bind to both hcp and top sites on Cu(111), our embedded MRSDCI calculations find that CO strongly prefers the top site, with CO not bound to the hcp site at all. This finding is consistent with experiment because CO binding to the threefold hollow site on Cu(111) is never observed. Thus, we see that when an ab initio theory incorporating the correct physics into the model is employed it is possible to get the correct description of the basic chemisorption phenomenon.

Acknowledgment. We are grateful to the Department of Energy, Basic Energy Sciences for support of this research. We would also like to thank Michele Pavone and Roland Lindh for useful discussions.

References and Notes

(1) Gajdos, M.; Eichler, A.; Hafner, J. *J. Phys. Condens. Matter* **2004**, *16*, 1141.
(2) Vollmer, S.; Witte, G.; Wöll, C. *Catal. Lett.* **2001**, *77*, 97.
(3) Steininger, H.; Lehwald, S.; Ibach, H. *Surf. Sci.* ***1982***, *123*, *264*.
(4) Smedh, H. A. B.; Borg, M.; Nyholm, R.; Anderson, J. N. *Surf. Sci.* **2001**, *491*, 115.
(5) Feibelman, P. J.; Hammer, B.; Norskov, J. K.; Wagner, F.; Scheffler, M.; Stumpf, R.; Watwe, R.; Dumesic, J. *J. Phys. Chem. B* **2001**, *105*, 4018.
(6) Olsen, R. A.; Philipsen, P. H. T.; Baerends, E. J. *J. Chem. Phys.* **2003**, *119*, 4522.
(7) Orita, H.; Itoh, N.; Inada, Y. *Chem. Phys. Lett.* **2004**, *3849*, 271.
(8) Neef, M.; Doll, K. *Surf. Sci.* **2006**, *600*, 1085.
(9) Doll, K. *Surf. Sci.* **2004**, *573*, 464.
(10) Aizawa, H.; Tsuneyuki, S. *Surf. Sci.* **1997**, *399*, L364.
(11) Blyholder, G. *J. Phys. Chem.* **1964**, *68*, 2772.
(12) Nilsson, A.; Wassdahl, N.; Weinelt, M.; Karis, O.; Wiell, T.; Bennich, P.; Hasselström, J.; Föhlisch, A.; Stöhr, J.; Sumant, M. *Appl. Phys. A* **1997**, *65*, 147.
(13) Ohnishi, S.; Watari, N. *Phys. Rev. B* **1993**, *49*, 14619.
(14) Gumhalter, B.; Wandelt, K.; Avouris, Ph. *Phys. Rev. B* **1988**, *37*, 8048.
(15) Gajdos, M.; Hafner, J. *Surf. Sci* **2005**, *590*, 117.
(16) Mason, S.; Grinberg, I.; Rappe, A. *Phys. Rev. B* **2004**, *69*, 161401.
(17) Hu, Q.-M.; Reuter, K.; Scheffler, M. *Phys Rev. Lett.* **2007**, *98*, 176103.
(18) Svensson, M.; Humbel, S.; Froese, R. D. J.; Matsubara, T.; Sieber, S.; Morokuma, K. *J. Phys. Chem.* **1996**, *100*, 19357.
(19) Govind, N.; Wang, Y. A.; de Silva, A. J. R.; Carter, E. A. *Chem. Phys. Lett.* **1998**, *295*, 129.
(20) Govind, N.; Wang, Y. A.; Carter, E. A. *J. Chem. Phys.* **1999**, *110*, 7677.
(21) Klüner, T.; Govind, N.; Wang, Y. A.; Carter, E. A. *Phys. Rev. Lett.* **2001**, *86*, 5954.
(22) Klüner, T.; Govind, N.; Wang, Y. A.; Carter, E. A. *J. Chem. Phys.* **2002**, *116*, 42.
(23) Klüner, T.; Govind, N.; Wang, Y. A.; Carter, E. A. *Phys. Rev. Lett* **2002**, *88*, 209702.
(24) Huang, P.; Carter, E. A. *Nano Lett.* **2006**, *6*, 1146.
(25) Huang, P.; Carter, E. A. *J. Chem. Phys.* **2006**, *125*, 084102.
(26) Perdew J. P.; Zunger, A. *Phys. Rev. B* **1981**, *23*, 5048.
(27) Perdew, J. P.; Burke, K.; Ernzerhof, M. *Phys. Rev. Lett.* **1996**, *77*, 3865.
(28) Monkhorst, H. J.; Pack, J. D. *Phys. Rev. B* **1976**, *13*, 5188.
(29) Segall, M. D.; Lindan, P. J. D.; Probert, M. J.; Pickard, C. J.; Hasnip, P. J.; Clark, S. J.; Payne, M. C. *J. Phys. Condens. Matter* **2002**, *14*, 2717.
(30) Huber, K. P.; Herzberg, G. *Molecular Spectra and Molecular Structure IV. Constants of Diatomic Molecules*; Van Nostrand Reinhold Co.: New York, 1979.
(31) Moler, E. J.; Keller, S. A.; Huff, W. R. A.; Hussain, Z. *Phys. Rev. B* **1996**, *54*, 10862.
(32) Stevens, W. J.; Basch, H.; Krauss, M. *J. Chem. Phys.* **1984**, *81*, 6026.
(33) Hay, P. J.; Wadt, W. R. *J. Chem. Phys.* **1985**, *82*, 270.
(34) Bagus, P. S.; Bauschlicher, C. W., Jr.; Nelin, C. J.; Laskowski, B. C.; Seel, M. *J. Chem. Phys.* **1984**, *81*, 3594.
(35) Siegbahn, P. E. M. *Lecture Notes in Quantum Chemistry*; Roos, B. O., Ed.; Springer-Verlag: Berlin, 1992; Vol. 58, p 255.
(36) Roos, B. O.; Taylor, P. R.; Siegbahn, P. E. M. *Chem. Phys.* **1980**, *48*, 157.
(37) Malmqvist, P.-Å.; Rendell, A.; Roos, B. O. *J. Phys. Chem* **1990**, *94*, 5477.
(38) Karlström, G.; Lindh, R.; Malmqvist, P.-Å.; Roos, B. O.; Ryde, U.; Veryazov, V.; Widmark, P.-O.; Cossi, M.; Schimmelpfennig, B.; Neogrady, P.; Seijo, L. *Comput. Mater. Sci.* **2003**, *28*, 222.
(39) Parr, R. G.; Yang, W. *Density Functional Theory of Atoms and Molecules*; International Series of Monographs on Chemistry; Oxford University Press: New York, 1989.
(40) Huang, P.; Carter, E. A., submitted.
(41) Hollins, P.; Pritchard, J. *Surf. Sci.* **1979**, *89*, 486−495.
(42) Kirstein, W.; Krueger, B.; Thieme, F. *Surf. Sci.* **1986**, *176*, 505.
(43) Kessler, J.; Thieme, F. *Surf. Sci.* **1997**, *67*, 405.
(44) Bartels, L.; Meyer, G.; Rieder, K.-H. *Surf. Sci.* **1999**, *432*, L621.
(45) Mochizuki, Y.; Tanaka, K.; Ohno, K.; Tatewaki, H. *Phys. Rev. B* **1989**, *39*, 11907.